



CrossMark
click for updates

Cite this: *RSC Adv.*, 2015, 5, 95939

Received 8th September 2015
Accepted 20th October 2015

DOI: 10.1039/c5ra18307c

www.rsc.org/advances

Enhancing photoresponsivity of self-powered UV photodetectors based on electrochemically reduced TiO₂ nanorods†

Pengli Yan,^{ab} Yihui Wu,^{ac} Guiji Liu,^{ac} Ailong Li,^{ac} Hongxian Han,^{*a} Zhaochi Feng,^a Jingying Shi,^a Yang Gan^{*b} and Can Li^{*a}

Electrochemically reduced TiO₂ nanorod arrays (R-NRAs) have been used for the first time to construct a self-powered, visible light blind ultraviolet (UV) photodetector. The fabricated R-NRAs device demonstrated superior photodetector performance with high photon-to-current efficiency of up to 22.5% at an applied bias of 0 V. The enhancement is attributed to a disordered surface layer which greatly improves the charge separation and transfer efficiency at the electrode/electrolyte interface.

UV detectors have been attracting substantial interest in recent years due to their application in fire detection, optical communication, environmental monitoring, UV astronomy, *etc.*^{1,2} Recent reports indicate that nanorod based detectors show excellent responsivity due to their unique properties, such as large surface-to-volume ratio and extended charge carrier lifetime.^{3–5} However, these photodetectors typically require an external bias to prevent the recombination of the photo-generated charge carriers, and the response time is extremely slow. The TiO₂ photoelectrochemical cell, which has the same structure as the conventional DSSCs but without dye adsorption, has been proposed to serve as a new type of self-powered photodetector with ultra-high responsivity and fast response time.^{6,7} Therefore, one-dimension (1D) TiO₂ nanostructures with wide bandgap (3.0 or 3.2 eV) and high stability may have great potential applications in UV detection. In such devices, electrode/electrolyte interface plays vital role in charge separation and transfer, and hence may drastically influence the performance of the detectors.^{8–10}

In the past few years, various strategies have been pursued to improve the performance of UV detectors, such as surface passivation and fabrication of heterojunctions.^{5,11–14} For example, it has been reported that TiO₂ nanowire coated with a thin polymer layer could significantly block the leakage current and hence induce extremely low dark current.⁵ The heterojunction structure with favourable band alignment has been also proposed to contribute to the higher ultraviolet sensitivity with enhanced photodetector performance.^{13,15,16} Clearly, these results from different strategies indicate that formation of a surface overlayer directly affects the charge separation and transfer.

The disordered TiO₂ with electronic defects may open up a new avenue for promoting charge transfer.^{17–19} Recently, we reported an electrochemical strategy for tuning the surface structure of TiO₂ nanorod arrays (NRAs).²⁰ It was found that the disordered surface layer not only improves the bulk charge separation but also suppresses the charge recombination at the electrode/electrolyte interface. In this work, such kind of TiO₂ with disordered surface layer (R-NRAs) is used to fabricate self-powered UV detector for the first time. Achievement of high UV responsivity demonstrates that TiO₂ with disordered surface layer is a desirable material for application in UV detector devices. And the negative shift of the surface band structure by the disordered surface layer is found to be responsible for achieving efficient charge separation and transfer at the electrode/electrolyte interfaces, hence dramatically improving the performance of the UV detector.

The NRAs were fabricated by a hydrothermal method as described in our previous work.²⁰ It can be seen from Fig. 1a and b that the as fabricated nanorods were about 100–150 nm in diameter and 3–3.5 μm in length, which were almost perpendicular to the FTO substrate. The reduced NRAs (R-NRAs) were prepared under –1.8 V (*vs.* SCE) in a typical three electrode system. The SEM images and the UV-vis spectra of NRAs and R-NRAs show no significant difference (Fig. S1, ESI†).

As shown in Fig. 1c, the HRTEM images of the NRAs indicated that the nanorods are single crystalline and the lattice

^aState Key Laboratory of Catalysis, Dalian Institute of Chemical Physics, Chinese Academy of Sciences, Dalian National Laboratory for Clean Energy, Dalian, 116023, China. E-mail: canli@dicp.ac.cn; hxhan@dicp.ac.cn; Tel: +86 411 84379070

^bSchool of Chemical Engineering & Technology, Harbin Institute of Technology, Harbin, 150001, China. E-mail: ygan@hit.edu.cn; Tel: +86 451 86413708

^cUniversity of Chinese Academy of Sciences, Beijing, 100049, China

† Electronic supplementary information (ESI) available: Experimental details and additional characterization data of the NRAs and R-NRAs are presented. See DOI: 10.1039/c5ra18307c

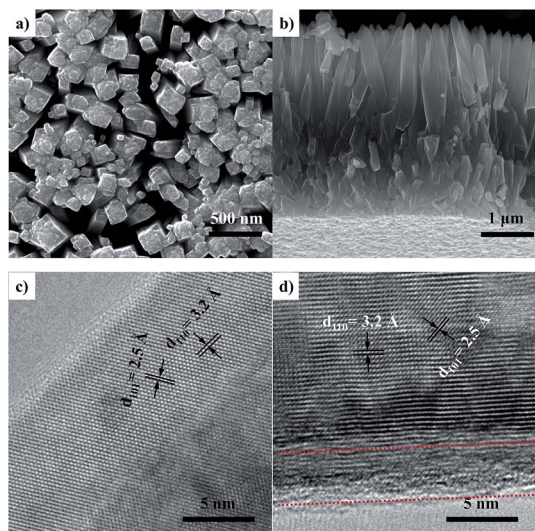


Fig. 1 SEM images of NRAs from top view (a) and cross-section view (b); HRTEM images of (c) NRAs and (d) R-NRAs.

fringes of 3.2 Å and 2.5 Å are attributed to the rutile (110) and (101) crystal planes respectively, which are consistent with the results from XRD pattern (Fig. S2, ESI[†]). After electrochemical reduction, the nanorods of the R-NRAs are capped with a disordered shell and the shell is about 4 nm (Fig. 1d). The distances between the adjacent lattice planes of the shell are no longer uniform, while the bulk shows well resolved (110) lattice plane with typical rutile plane distance (Fig. S3[†]). The thickness of the disordered layer can be tuned by varying the electrochemical reduction bias voltage and reaction time.²⁰ Thus, we speculate that the formation of the disordered surface layer is due to the electrochemical reduction.

The J - V curves (Fig. 2a) show that the device has good photovoltaic response. Two significant features were observed from these curves: firstly, the short circuit current density (J_{sc}) of the R-NRAs device is 7.44 mA cm⁻², which is 2.4 times of that of the NRAs device (3.11 mA cm⁻²). Secondly, the open circuit voltage (V_{oc}) of the R-NRAs is 0.16 V higher than that of the NRAs device, which can be attributed to the negative shift of the Fermi level of the R-NRAs compared to that of the NRAs (Fig. S4, ESI[†]).

This allows rapid hole accumulation at the disordered surface layer and prevent recombination of photoexcited charge carriers in the nanorods.

The time-resolved photocurrent response of the NRAs and R-NRAs devices were investigated over several switching on/off cycles under weak illumination with 385 nm LED (4 mW cm⁻²) at a bias of 0 V. As shown in Fig. 2b, the photocurrent of the R-NRAs device could reach 0.39 mA cm⁻² while that of the NRAs device is about 0.24 mA cm⁻². The uniform, stable and rectangular-shaped current response of both devices is an indication that the devices are stable within a certain time. The corresponding current density rise and decay times are presented in Fig. 2c. It can be seen that the rise time (the time of dark current to 90% of maximum photocurrent) and decay time (the time of photocurrent to 10% of maximum photocurrent) of R-NRAs is less than 3 ms, smaller than that of 4 ms of NRAs. The faster response of the device might be due to the promotion of charge transfer by the electronic defects in the disordered surface layer of R-NRAs.^{17,20}

The photosensitivity of the device to 385 nm UV light was measured under a series of irradiation power ranging from 0.03 to 85 mW cm⁻² (Fig. S5, ESI[†]). As shown in Fig. 3a, the photocurrents are almost linearly increased with the increase of the illumination intensity, which suggests that the devices can be used to sense the UV light intensity. The maximum responsivity of the R-NRAs is more than 0.09 A/W while that of the NRAs device is about 0.055 A/W. Moreover, the R-NRAs device achieves a responsivity of more than 0.07 A W⁻¹ under irradiation power at the range of 1.5–85 mW cm⁻².

The UV selectivity of the devices were checked with IPCE and the corresponding results are presented in Fig. 3b. It can be seen that the spectral response of the two devices are in the same range of 310–420 nm, which is due to the intrinsic absorption edge of the TiO₂ that restricts the absorbed photons to a minimum energy of 3.0 eV (Fig. S1, ESI[†]). But the R-NRAs device shows much higher UV responsive efficiency than that of the NRAs device. At the maximum responsive wavelength of 380 nm, the photon-to-current efficiency of the R-NRAs device is *ca.* 22.5% while that of the NRAs device is only *ca.* 10.3%. These results indicate that the photoconversion efficiency is improved in the entire UV region.

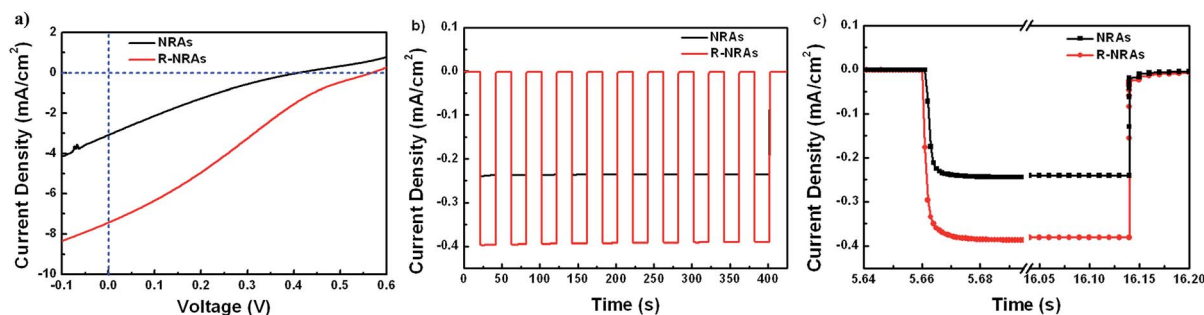


Fig. 2 (a) J - V curves of NRAs and R-NRAs devices under 385 nm UV light illumination (90 mW cm⁻²); (b) current response of NRAs and R-NRAs devices under on/off radiation of 4 mW cm⁻² of 385 nm UV light; (c) the magnified curves showing the rise and decay edges of the current response.

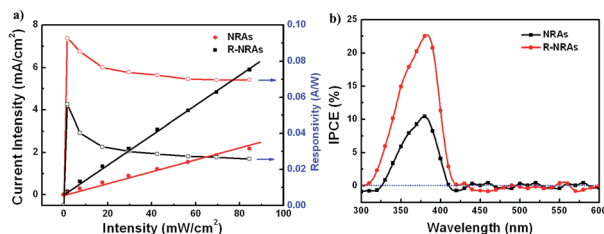


Fig. 3 (a) The photocurrent response and the relative responsivity of the NRAs and R-NRAs devices measured under 385 nm UV light illumination; (b) IPCE of the NRAs and R-NRAs devices in the wavelength range of 300–600 nm.

In order to better understand the superior responsivity of the R-NRAs device, electrochemical independence spectroscopy (EIS) has been applied to study the charge transfer properties at the electrode/electrolyte interface. Fig. 4a shows the Bode plots of the NRAs and R-NRAs devices tested under 385 nm LED light illumination (4 mW cm^{-2}) with a bias equal to V_{oc} . The low impedance of the R-NRAs device indicates that it has low charge transfer resistance. The effective life time of electrons can be calculated with the following approximate equation:²¹

$$\tau_{\text{eff}} \approx \frac{1}{\omega_{\text{min}}} = \frac{1}{2\pi f_{\text{min}}}$$

where τ_{eff} is the effective life time of electrons, ω_{min} is the minimum angular frequency and f_{min} is the corresponding frequency. The calculated τ_{eff} of the NRAs and R-NRAs are 60 ms and 197 ms, respectively. Apparently, the disordered surface layer greatly extended the life time of electrons.

To gain better understanding on the charge transfer mechanism, the band structure analysis has been carried out. The negative shift of the flat band position (Fig. S4, ESI†) indicates that the conduction band of the disordered surface layer has lower electron affinity than that of the bulk rutile. As revealed by the same absorption edge positions of NRAs and R-NRAs in UV-vis spectra (Fig. S1, ESI†), the valence band position of the disordered surface layer should be more negative than that of the bulk rutile. Moreover, large amounts of lattice disorder in the surface layer could yield mid-gap states near the conduction band and valence band.¹⁸ The increased visible region absorption may be stemmed from the electrons excited from the shallow state energy levels in the disordered surface layer.²⁰

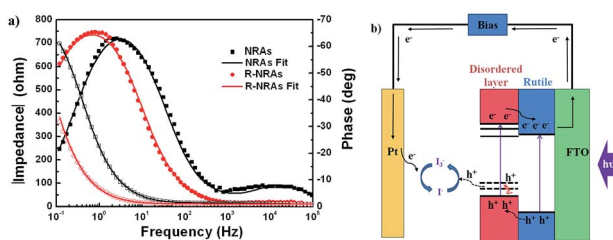


Fig. 4 (a) EIS measurements under 385 nm UV illumination with a bias of V_{oc} ; (b) representation of the disordered surface layer approach for UV detection.

Hence, the migration route of the photogenerated charge carriers in the R-NRAs device can be plausibly illustrated as shown in Fig. 4b. Obviously, formation of such kind of staggered band alignments may facilitate not only electron transfer from the surface to the bulk of the TiO_2 but also hole accumulated in the disordered surface layer. Moreover, the electronic defects in the disordered surface layer would promote the hole conduction and sufficiently suppress the charge recombination.¹⁷ Overall, the R-NRAs with the disordered surface layer can achieve more efficient charge separation and hence enhance the responsivity and reduce the response time.

In summary, we have developed a self-powered, simple and convenient UV detector which is consisted of TiO_2 nanorod arrays with disordered surface layer (R-NRAs). The device shows a high responsivity of more than 0.09 A/W under 385 nm UV illumination at the intensity of 1.6 mW cm^{-2} . The dramatic improvement of the performance of R-NRAs device compared to that of the RNAs is due to the enhancement of charge separation and transfer at the electrode/electrolyte interfaces by the negative shift of the surface band structure of R-NRAs, which is caused by the introduction of the disordered surface layer. This work demonstrates that surface properties of semiconductor play an important role in its corresponding devices. Construction of disordered surface layer may greatly improve the charge separation and transfer efficiency at the electrode/electrolyte interface, which may be also a suitable strategy for the assembly of TiO_2 based DSSCs and lithium ion batteries.

Acknowledgements

This work has been supported by the National Natural Science Foundation of China (No. 21473189), the National Basic Research Program of China (973 Program, Grant No. 2014CB239401), the Key Research Program of the Chinese Academy of Science (Grant No. KGZD-EW-T05), the Fundamental Research Funds for the Central Universities (No. HIT. KISTP.201406), and the Collaborative Innovation Center of Chemistry for Energy Materials (iChem).

Notes and references

- 1 H. Morkoc, S. Strite, G. B. Gao, M. E. Lin, B. Sverdlov and M. Burns, *J. Appl. Phys.*, 1994, **76**, 1363.
- 2 W. Tian, H. Lu and L. Li, *Nano Res.*, 2015, **8**, 382.
- 3 S. N. Das, K.-J. Moon, J. P. Kar, J.-H. Choi, J. Xiong, T. I. Lee and J.-M. Myoung, *Appl. Phys. Lett.*, 2010, **97**, 022103.
- 4 C. Yan and P. S. Lee, *Sci. Adv. Mater.*, 2012, **4**, 241.
- 5 M. Zhang, D. Li, J. Zhou, W. Chen and S. Ruan, *J. Alloys Compd.*, 2015, **618**, 233.
- 6 X. Li, C. Gao, H. Duan, B. Lu, X. Pan and E. Xie, *Nano Energy*, 2012, **1**, 640.
- 7 Z. Wang, S. Ran, B. Liu, D. Chen and G. Shen, *Nanoscale*, 2012, **4**, 3350.
- 8 G. Liu, J. Shi, F. Zhang, Z. Chen, J. Han, C. Ding, S. Chen, Z. Wang, H. Han and C. Li, *Angew. Chem., Int. Ed.*, 2014, **53**, 7295.

- 9 E. Palomares, J. N. Clifford, S. A. Haque, T. Lutz and J. R. Durrant, *J. Am. Chem. Soc.*, 2002, **125**, 475.
- 10 M. Matsukawa, R. Ishikawa, T. Hisatomi, Y. Moriya, N. Shibata, J. Kubota, Y. Ikuhara and K. Domen, *Nano Lett.*, 2014, **14**, 1038.
- 11 X. Li, C. Zhu, X. Zhu, Z. Xu, X. Zhuang, X. Ji and F. Yan, *Appl. Phys. Lett.*, 2013, **103**, 171110.
- 12 O. Game, U. Singh, T. Kumari, A. Banpurkar and S. Ogale, *Nanoscale*, 2014, **6**, 503.
- 13 Y. Bie, Z. Liao, H. Zhang, G. Li, Y. Ye, Y. Zhou, J. Xu, Z. Qin, L. Dai and D. Yu, *Adv. Mater.*, 2011, **23**, 649.
- 14 X. Hou, X. Wang, B. Liu, Q. Wang, Z. Wang, D. Chen and G. Shen, *ChemElectroChem*, 2014, **1**, 108.
- 15 S. M. Hatch, J. Briscoe and S. Dunn, *Adv. Mater.*, 2013, **25**, 867.
- 16 M. Shasti, A. Mortezaali and R. S. Dariani, *J. Appl. Phys.*, 2015, **117**, 023101.
- 17 S. Hu, M. R. Shaner, J. A. Beardslee, M. Lichterman, B. S. Brunshwig and N. S. Lewis, *Science*, 2014, **344**, 1005.
- 18 X. Chen, L. Liu, P. Y. Yu and S. S. Mao, *Science*, 2011, **331**, 746.
- 19 T. Xia, W. Zhang, J. Murowchick, G. Liu and X. Chen, *Nano Lett.*, 2013, **13**, 5289.
- 20 P. Yan, G. Liu, C. Ding, H. Han, J. Shi, Y. Gan and C. Li, *ACS Appl. Mater. Interfaces*, 2015, **7**, 3791.
- 21 R. Kern, R. Sastrawan, J. Ferber, R. Stangl and J. Luther, *Electrochim. Acta*, 2002, **47**, 4213.